Original papers
Materials for energy and environment, next-generation photovoltaics, and green technologies

УДК 544.6.076+544.6.018.47-039.7+544.636/.638 DOI: 10.17277/jamt-2026-11-02-139-151

Supercapacitors based on graphene nanoflakes and redox-active ferrocene-containing ionic liquids

© Mikhail M. Levin[a]✉, Ekaterina A. Arkhipova[a], Anton S. Ivanov[a], Konstantin I. Maslakov[a], Serguei V. Savilov[a]

[a] *Lomonosov Moscow State University, Faculty of Chemistry, Leninskie gory, Bld. 3, 1, Moscow, 119234, Russian Federation*
✉ mikhail.levin@chemistry.msu.ru

Abstract. A series of ferrocene-containing ionic liquids (Fc-ILs) (bis(trifluoromethylsulfonyl)imides ofN-methyl-N-(ferrocenylmethyl)pyrrolidinium, N-methyl-N-(ferrocenylmethyl)piperidinium and N-ethyl-N-(ferrocenylmethyl) pyrrolidinium) were tested as redox-active additives for supercapacitor (SC)ionic liquid electrolytes. Undoped and nitrogen-dopedgraphene nanoflakes (GNFs) were used as an electrode material. The electrochemical characteristics of SCs were analyzed bycyclic voltammetry (CV), galvanostatic charge-discharge (GCD) and electrochemical impedance spectroscopy. Self-discharge of SCs was measured at open-circuit potential. The specific capacitance, energy density, Coulombic efficiency and self-discharge of the SCs depended on the textural parameters of the electrode material and type and content of the additive to the electrolyte. The increase in the Fc-IL fraction in the 0.5 M [EMIm][NTf_2]/ acetonitrile supporting electrolyte enhanced the specific capacitance of the GNF-based electrode from 85 to 126 $F \cdot g^{-1}$ at a scan rate of 5 $mV \cdot s^{-1}$ due to additional pseudocapacitive contribution from reversible electron transfer in Fe^{2+}/Fe^{3+}. Moreover, the redox-active additives provided the increase in energy density of the SC up to 21.7 $Wh \cdot kg^{-1}$. Nitrogen doping of GNF accelerated the self-discharge due to the interaction between redox-active species and nitrogen groups on the electrode surface.

Keywords: supercapacitors; graphene nanoflakes; redox-active electrolytes; ferrocene; ionic liquids.

For citation: Levin MM, Arkhipova EA, Ivanov AS, Maslakov KI, Savilov SV. Supercapacitors based on graphene nanoflakes and redox-active ferrocene-containing ionic liquids. *Journal of Advanced Materials and Technologies*. 2026;11(2):139-151. DOI: 10.17277/jamt-2026-11-02-139-151

Суперконденсаторы на основе малослойных графитовых фрагментов и редокс-активных ферроценсодержащих ионных жидкостей

© М. М. Левин[a]✉, Е. А. Архипова[a], А. С. Иванов[a], К. И. Маслаков[a], С. В. Савилов[a]

[a] *Московский государственный университет им. М. В. Ломоносова, Химический факультет, ул. Ленинские горы, 1, стр. 3, Москва, 119234, Российская Федерация*

✉ mikhail.levin@chemistry.msu.ru

Аннотация. Ферроценсодержащие ионные жидкости (Fc-ИЖ) (бис(трифторметилсульфонил)имиды N-метил-N-(ферроценилметил)пирролидиния, N-метил-N-(ферроценилметил)пиперидиния и N-этил-N-(ферроценилметил) пирролидиния) испытаны в качестве окислительно-восстановительных добавок для электролитов суперконденсаторов (СК). В качестве электродного материала изучены малослойные графитовые фрагменты (МГФ), в том числе азотзамещённые (N-МГФ). Анализ электрохимических характеристик СК проведен с помощью методов циклической вольтамперометрии, гальваностатического заряда-разряда и спектроскопии электрохимического импеданса. Саморазряд СК измерен при потенциале холостого хода. Показано, что пористые параметры электродного материала, тип и содержание редокс-добавки в электролите определяют удельную ёмкость, плотность энергии, кулоновскую эффективность и величину саморазряда СК. Установлено, что увеличение доли Fc-ИЖ в фоновом электролите 0,5 М [EMIm][NTf_2]/ацетонитрил приводит к увеличению удельной емкости электрода на основе МГФ с 85 до 126 Ф/г при скорости развертки потенциала 5 мВ/с за счет дополнительного псевдоемкостного вклада, обусловленного обратимым переносом электронов в ходе редокс-

процесса Fe^{2+}/Fe^{3+}, а также способствует росту удельной энергии СК до 21,7 Вт/кг. В отличие от МГФ, легирование азотом оказывает негативное влияние на электрохимические характеристики СК, приводя к ускорению саморазряда вследствие взаимодействия редокс-активных частиц с азотными группами на поверхности электрода.

Ключевые слова: суперконденсаторы; малослойные графитовые фрагменты; редокс-активные электролиты; ферроцен; ионные жидкости.

Для цитирования: Levin MM, Arkhipova EA, Ivanov AS, Maslakov KI, Savilov SV. Supercapacitors based on graphene nanoflakes and redox-active ferrocene-containing ionic liquids. *Journal of Advanced Materials and Technologies*. 2026;11(2):139-151. DOI: 10.17277/jamt-2026-11-02-139-151

1. Introduction

The rapid expansion of the global economy leads to depletion of fossil fuels and accelerates anomalous climate change. This makes the development of clean renewable energy solutions the key task of modern industries. Nowadays, different energy storage technologies, such as supercapacitors (SCs), metal-ion batteries and fuel cells have been rapidly growing. Among them SCs stand out by fast charge/discharge rates, cycling stability, high-power density and low cost [1, 2]. However, compared to Li-ion batteries the commercially available SCs release lower specific energy density that is about 5–15 $Wh \cdot kg^{-1}$ [3]. The increase in the specific capacitance C and potential range V allows enhancing the SC energy density calculated as $E_{SC} = 0.5CV^2$ [4]. The use of redox-active electrode materials or electrolytes is a successful strategy to improve the specific capacitance of SCs due to additional pseudocapacitive contribution caused by reversible Faradaic reactions [5, 6].

Over a decade, different metal oxides [7, 8], conducting polymers (polyaniline, polythiophene, polypyrrole, etc.) [9], and modified carbon nanomaterials [10] have been applied as electrode materials of SCs. Carbon-based nanomaterials are of particular interest due to their chemical stability, developed porosity and low cost. The introduction of heteroatoms, such as nitrogen, sulfur, oxygen, phosphorus and boron, into graphene layers changes their electronic structure, magnetic, optical and electrochemical properties [11]. In particular, N-doping enhances electrochemical activity of the electrode material because higher electronegativity of nitrogen atoms and their additional lone electron pairs improve its electrical conductivity [11] and enable efficient charge storage [12]. Sliwak et al. [12] showed that pseudocapacitance contribution increased the specific capacitance of reduced graphene oxide from 142 up to 209 $F \cdot g^{-1}$ at a current density of 20 $F \cdot g^{-1}$ in 6 M KOH. Similarly, a 300-fold enhancement in specific capacitance of pristine graphite in 1 M KOH was reported after doping of the electrode material with nitrogen.

The choice of electrolyte is crucial for the electrochemical performance of the SC. Currently, various aqueous and organic systems are widely used in SCs because of their high ionic conductivities and good interface wettability. Several redox-active electrolyte additives such as $K_3Fe(CN)_6$ [13–15], $K_4Fe(CN)_6$ [16], KI [17, 18], KBr [19, 20], $VOSO_4$ [17, 21], hydroquinone (HQ) [22, 23] have been reported. These additives provide extra redox pairs that boost charge storage via electron exchange. In contrast to electrode material engineering, tuning the electrolyte offers a more facile and cost-effective route to high pseudocapacitance. However, the potential operating window of SCs based on aqueous electrolytes is thermodynamically limited (< 1.23 V) by water decomposition [24]. Furthermore, freezing of aqueous electrolytes limits their applicability at extremely low temperatures. Replacement of aqueous solutions with ionic liquids (ILs) helps to overcome these limitations.

ILs are salts composed of organic cations and organic or inorganic anions. They are distinguished by negligible flammability and volatility, high thermal stability, and a wide operational temperature range [25, 26]. Moreover, a wide electrochemical stability window of ILs (up to 5–6 V [26]) enables higher energy densities of SCs. In recent years, a few redox-active ILs including 1-butyl-3-methylimidazolium iodide (BMIMI) [27], 1-butyl-3-methylimidazolium bromide (BMIMBr) [28, 29], N-butyl-N-methylpyrrolidinium bromide ($Pyr_{14}Br$) [30], dimethyl-1,1’-bis(N-butylimidazolium)ferrocene chloride [31], 1-ethyl-3-methylimidazolium ferrocenylsulfonyl-(trifluoromethylsulfonyl)-imide ([Emim][FcNTf]) [32], N-6-ferrocenehexyl-N’-methylimidazolium bis(trifluoromethanesulfon)imide [33], N-2-ethylhexyl-N′-isopentyl-4,4′-bipyridinium bis(di(trifluoromethanesulfon)imide) [33] and 1-methyl-3-(3-((2,2,6,6-tetramethylpiperidin-4-yl)oxy) propyl)-1H-imidazol-3-ium

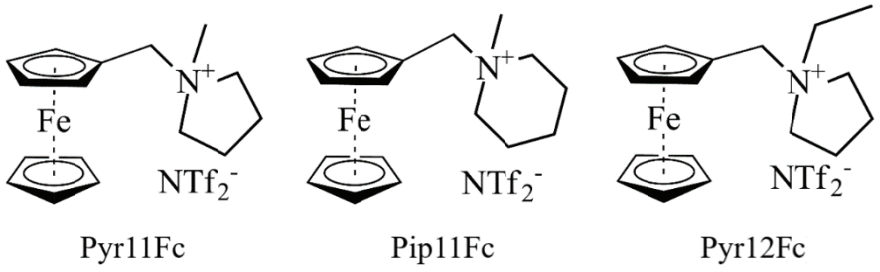

Fig. 1. Fc-ILs used as redox-active electrolyte additives

bis(trifluoromethanesulfon)imide [33] have been tested as SC electrolytes. Fan et al. [28] found that a pseudocapacitance contribution from a Br^-/Br_3^-. Faradaic reaction at the electrode/electrolyte interface increased the specific capacitance from 65.3 to 392 $F \cdot g^{-1}$ at 0.25 $A \cdot g^{-1}$, and enhanced the energy density of the quasi-solid-state SC from 7.1 to 43.1 $Wh \cdot kg^{-1}$ [28]. Similarly, replacing the poly(vinyl alcohol) (PVA)/Li_2SO_4/BMIMCl electrolyte with a PVA/Li_2SO_4/BMIMI-based one increased the specific capacitance from 139.1 to 384.1 $F \cdot g^{-1}$ at a current density of 0.25 $A \cdot g^{-1}$ [27]. 80 wt. % solution of [Emim][FcNTf] in acetonitrile demonstrated higher specific energy of the SC (up to 13.2 $Wh \cdot kg^{-1}$) in the potential range of 2 V than the same solution of [Emim][NTf_2] (7.2 $Wh \cdot kg^{-1}$) [32]. Among redox-active ILs, ferrocene-based ILs (Fc-ILs) are considered as promising electroactive electrolytes due to the good solubility, high chemical and electrochemical stability, wide availability, and low cost of ferroceneprecursor [34]. The redox behavior of Fc-ILs originates from the reversible electron transfer in the Fe^{2+}/Fe^{3+} couple during charge/discharge cycles that provides pseudocapacitance.

Herein, the earlier synthesized Fc-ILs [35] (N-methyl-N-(ferrocenylmethyl)pyrrolidinium bis(trifluoromethylsulfonyl)imide (Pyr11Fc), N-methyl-N-(ferrocenylmethyl)piperidinium bis(trifluoromethylsulfonyl)imide (Pip11Fc), N-ethyl-N-(ferrocenylmethyl)pyrrolidinium bis(trifluoromethylsulfonyl)imide (Pyr12Fc)) (Fig. 1) were tested in SCs as redox-active electrolyte additives to enhance their electrochemical performance.

The aim of this study was to evaluate the effect of redox-active additives combined with graphene nanoflakes (GNFs) and nitrogen-doped GNFs electrodes on specific capacitance, self-discharge, energy and power densities of SCs.

2. Materials and Methods

The synthesis and characterization of Pyr11Fc, Pyr12Fc and Pip11Fc are described in detail in [35]. Redox-active solutions containing 0.01, 0.03 and 0.05 M Fc-ILs with a 0.5 M [EMIm][NTf_2] supporting electrolyte in acetonitrile (AN) (Sigma-Aldrich, ≥ 99.9 %) were prepared in an argon-filled glove box (water content < 0.1 ppm). A blank 0.5 M [EMIm][NTf_2] solution in AN was used as a reference additive-free electrolyte. GNFs (S_{BET} = = 1720 $m^2 \cdot g^{-1}$) [36] and N-GNFs ($[N]_{XPS}$ = 8.8 at. %, S_{BET} = 1180 $m^2 \cdot g^{-1}$) [37] were used as electrode materials. To prepare the slurry, 160 mg of the electrode material, 20 mg of conductive carbon black (Super C65, MTI Corporation) and 33 mg of a 60 wt. % polytetrafluoroethylene (PTFE) aqueous dispersion (MTI Corporation) were thoroughly mixed in ethanol using an agate mortar with a pestle. Then, a homogeneous paste was passed through a roller press and coated onto a nickel foam disk (d = 1 cm, porosity 98 %, MTI Corporation) used as a current collector. Afterwards, the electrodes were dried at a vacuum oven at 60 °C for 24 hours to remove moisture impurities. The coated paste area was 0.785 cm^2 with a mass loading of active material of ~7 $mg \cdot cm^{-2}$ (GNFs) and ~16 $mg \cdot cm^{-2}$ (N-GNFs).

Electrochemical measurements were carried out on a Biologic VSP potentiostat-galvanostat (Bio-Logic Science Instruments SAS, France). The SC was assembled in a 2032 coin-cell configuration with two identical electrodes separated by a glass microfiber filter (Whatman). Electrolyte volume corresponded to 140 μL. Cyclic voltammetry (CV) curves were recorded at a scan rate v of 5, 10, 20, 50, 100 and 200 $mV \cdot s^{-1}$ in the potential range of 0–2.5 V that corresponded the electrochemical stability windows of individual components of the electrolytes [35, 38]. Galvanostatic charge/discharge cycling was conducted at a current density i of 1, 1.5, 2, 2.5 $A \cdot g^{-1}$. The specific capacitances of the single electrode C_{CV} and C_{GCD} ($F \cdot g^{-1}$) and the SC cell C_{SC} were calculated from a discharge curve as [39]:

$$C_{CV} = \frac{4}{2m\Delta V v}\int_0^t IdV(t); \quad (1)$$

$$C_{GCD} = 4C_{SC} = 4\frac{2i\int Vdt}{(\Delta V)^2}, \quad (2)$$

where V is potential, V; I is current, A; and m is mass of active electrode material, g. The energy E_{SC} (Wh·kg^{-1}) and power P_{SC} (kW·kg^{-1}) densities were determined as:

$$E_{SC} = \frac{C_{GCD}\,\Delta V^2}{8\times 3.6}; \quad (3)$$

$$P_{SC} = \frac{E_{SC}}{t/3.6}, \quad (4)$$

where t is the discharge time, s.

The SCs were studied by electrochemical impedance spectroscopy in the frequency range from 10 MHz to 1 MHz with a potential amplitude of 10 mV around the open circuit potential of the discharged state.

To evaluate self-discharge of the SCs, the cells were charged up to 2.5 V at a scan rate of 10 mV·s^{-1} and kept at this potential for 60 s. Then, the open-circuit voltage was recorded for 5 h.

3. Results and Discussion

Figure 2 shows the CV curves recorded at a scan rate of 50 mV·s^{-1} for different concentrations of Fc-ILs in 0.5 M [EMIm][NTf$_2$]. The CV curves for the SCs with the blank electrolyte exhibit nearly rectangular response attributed to the charge accumulation through the electrochemical double-layer formation under adsorption of charge carriers at the electrode/electrolyte interface. In contrast, addition of the Fc-ILs to the electrolytes results in the appearance of reversible oxidation/reduction peaks attributing to the Fe^{3+}/Fe^{2+} redox reaction. The redox peaks became more pronounced with increasing the Fc-IL concentration (Fig. 2*b*) indicating the enhanced pseudocapacitance contribution.

For each Fc-IL additive the CV curve for 0.05 M Fc-IL electrolyte exhibited the highest current density. At a scan rate of 5 mV·s^{-1} the specific capacitances of GNF-electrodes in the electrolytes with additives were 126 (Pyr11Fc), 123 (Pyr12Fc) and 122 (Pip11Fc) F·g^{-1}, which were well above 85 F·g^{-1} observed for the blank electrolyte (Table 1). Even at a scan rate of 200 mV·s^{-1} the specific capacitance retained high values of 101 (Pyr11Fc), 99 (Pyr12Fc) and 97 (Pip11Fc) F·g^{-1} compared to 73 F·g^{-1} for the blank electrolyte. The decrease in the capacitance with increasing the scan rate is caused by the kinetic limitations due to the lack of time for charge carriers to penetrate into the porous electrode structure [40, 41].

N-GNFs showed similar to GNFs specific capacitances of 120 (0.05 MPyr11Fc), 118 (0.05 MPyr12Fc), 125 (0.05 MPip11Fc) and 101 (blank electrolyte) F·g^{-1} at 5 mV·s^{-1}. However, the increase in the scan rate resulted in a more pronounced dropin the specific capacitances of N-GNFs (Table 1). At 50 mV·s^{-1} the contribution of redox peaks to the CV area for N-GNFs electrodes is lower (Fig. 2*c*), which may be attributed to their significantly different porosity. The GNFs specific surface area of 1720 m^2·g^{-1} and mesopore volume of 2.38 cm^3·g^{-1} [36] are significantly higher than those of N-GNFs (1180 m^2·g^{-1} and 1.16 cm^3·g^{-1} [37]). The abundant mesopores in the electrode material should shorten the ion diffusion pathways and facilitate smooth and high-rate ion mobility [42]. Therefore, higher free pore volume of GNFs provided by mesopores reduces the kinetic limitations for charge carriers during charging/discharging processes. In contrast, lower fraction of mesopores and a high content of micropores (0.54 cm^3·g^{-1}) in N-GNFs can impede migration of bulk solvated ions of Fc-ILs into the porous electrode structure. These limitations become more pronounced at higher scan rates. Thus, the difference in the GNFs and N-GNFs porosity was expected to result in their different electrochemical performances in SCs. Nevertheless, the similar values of specific capacitances of these electrodes at low scan rates suggest that lower double layer capacitance of N-GNFs because of their lower specific surface area is compensated by extra pseudocapacitive contribution provided by reversible redox reactions that involve nitrogen species in N-GNF. However, this compensation effect diminishes at higher scan rates. At 200 mV·s^{-1} the specific capacitances of N-GNFs were lower than those of GNFs:76 (Pyr11Fc), 72 (Pyr12Fc), 81 (Pip11Fc) and 74 (blank electrolyte) F·g^{-1}.

The non-linearity of the GCD curves recorded for Fc-ILs-electrolytes confirms the Faradaic behavior of redox-active electrolytes (Figs. 2*d–f*). The GCD results demonstrate that the GNFs-based electrodes combined with redox-additives of the electrolytes provide higher capacitances than the N-GNFs electrodes (Table 2), which agrees with the CV data (Table 1).

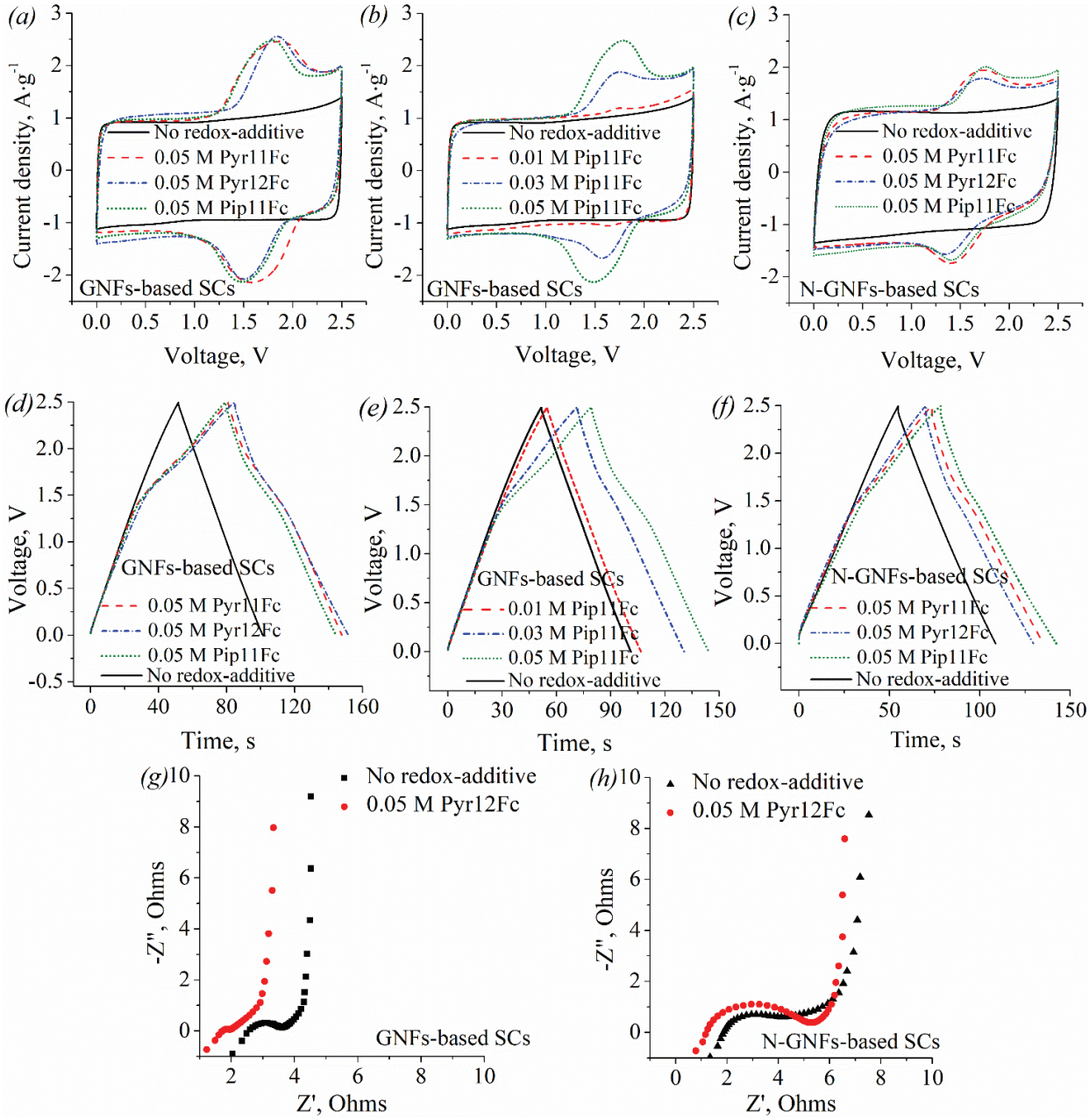

Fig. 2. CV (*a* – *c*) and GCD (*d* – *f*) curves of GNFs- (*a*, *b*, *d*, *e*) and N-GNFs- (*c*, *f*) based SCs recorded at scan rate of 50 mV·s^{-1} and current density of 1 A·g^{-1} (Potential range = 0 – 2.5 V, T = 298 K). Nyquist plots for GNFs- (*g*) and N-GNFs-based SCs (*h*) with 0.5 M [EMIm][NTf_2]/AN + 0.05 M Pyr12Fc

However, in the blank electrolyte the specific capacitance of N-GNFs (90.1 F·g^{-1} at 1 A·g^{-1}) exceeded this value for GNFs (79.6 F·g^{-1} at 1 A·g^{-1}). These results point to specific interactions between surface nitrogen-species and redox-active additives that reduce electrochemical performance of the SC. In particular, nitrogen groups may enhance the adsorption of products forming in a Faradaic process on the carbon electrode and increase self-discharge. The 0.05M Pyr11Fc additive to supporting electrolyte 0.5 M [EMIm][NTf_2]/AN provided slightly higher specific capacitance of GNFs (108.3 F·g^{-1} at 1 A·g^{-1}) than 0.05M Pyr12Fc(107.3 F·g^{-1}) and 0.05M Pip11Fc (104.6 F·g^{-1}) ones. The unit cell volume of the crystals increases in the series Pyr11Fc (1156.96(14) Å^3) < Pyr12Fc (2407.1(3) Å^3) < Pip11Fc (4771.6(5) Å^3) [35]. The lowest volume of Pyr11Fc is favorable for ions migration inside the smallest inner pores of the electrode. Indeed, the ionic conductivity of Fc-ILs in AN with a molar fraction of $x_{Fc\text{-IL}}$ = = 0.05 at 298.15 K follows the decreasing order: Pyr11Fc ((26.25 ± 0.28) mS·cm^{-1}) > Pyr12Fc ((25.79 ± ± 0.31) mS·cm^{-1}) > Pip11Fc ((23.94 ± 0.30) mS·cm^{-1}) [35].

Table 1. Effect of redox-active additives on specific capacitances ($F \cdot g^{-1}$) of GNF- and N-GNF-based electrodes at different scan rates

v, $mV \cdot s^{-1}$	GNFs						N-GNFs					
	5	10	20	50	100	200	5	10	20	50	100	200
No additive	85	83	81	78	76	73	101	97	93	88	83	74
0.01M Pyr11Fc	99	97	93	88	84	80	111	106	101	94	86	74
0.03M Pyr11Fc	112	109	106	101	96	90	116	110	104	94	89	64
0.05M Pyr11Fc	126	121	117	112	107	101	120	114	109	100	90	76
0.01M Pyr12Fc	93	91	89	85	82	78	105	99	95	88	81	71
0.03M Pyr12Fc	119	117	114	109	105	99	114	107	102	94	85	72
0.05M Pyr12Fc	123	119	115	109	102	93	118	113	106	95	85	71
0.01M Pip11Fc	93	91	88	84	81	78	104	97	92	84	76	65
0.03M Pip11Fc	110	107	103	97	90	83	117	112	105	92	80	65
0.05M Pip11Fc	122	119	115	109	104	97	125	119	113	104	95	81

Table 2. Effect of redox-active additives on specific capacitances ($F \cdot g^{-1}$) of GNF- and N-GNF-based electrodes at different current densities

i, $A \cdot g^{-1}$	GNFs				N-GNFs			
	1	1.5	2	2.5	1	1.5	2	2.5
No additive	79.6	74.6	78.2	72.4	90.1	88.2	86.5	85.0
0.01M Pyr11Fc	90.5	80.5	88.1	78.0	95.4	93.0	90.7	88.6
0.03M Pyr11Fc	92.6	89.2	91.8	87.3	95.9	92.5	88.7	85.1
0.05M Pyr11Fc	108.3	106.2	106.7	104.2	100.4	98.1	95.6	93.1
0.01M Pyr12Fc	86.6	79.5	84.3	76.8	89.4	86.9	84.8	82.8
0.03M Pyr12Fc	103.6	97.5	103.5	96.0	94.4	92.2	89.8	87.5
0.05M Pyr12Fc	107.3	98.5	106.6	95.0	84.7	85.0	89.1	91.4
0.01M Pip11Fc	83.3	77.2	81.8	75.0	85.4	82.5	80.0	77.6
0.03M Pip11Fc	95.1	86.5	92.5	83.2	92.3	90.7	88.0	85.0
0.05M Pip11Fc	104.6	99.6	103.4	97.3	103.9	101.8	99.5	97.2

This trend correlates with the mobility of the cations: the diffusion coefficients determined for 0.01 M Fc-IL solutions in AN were $5.06 \cdot 10^{-6}$ $cm^2 \cdot s^{-1}$ ($Pyr11Fc^+$), $4.76 \cdot 10^{-6}$ $cm^2 \cdot s^{-1}$ ($Pyr12Fc^+$), and $4.51 \cdot 10^{-6}$ $cm^2 \cdot s^{-1}$ ($Pip11Fc^+$) [35].

The results are consistent with the electrochemical impedance spectroscopy data (Fig. 2*g*, *h*). The charge transfer resistance (R_{ct}), defined by the diameter of the semicircle, is the smallest for GNFs-based SCs. In contrast, N-GNFs-based SCs demonstrate a higher R_{ct} value, which is attributed to diffusion limitations caused by ion migration within the porous electrode structure during charge storage.

GCD curves were also used to study the effect of self-discharge due to the so-called "shuttle effect" – diffusion of the redox component to the opposite electrode immediately after oxidation/reduction [43]. Because of this effect the charge capacity exceeds the discharge capacity. The ratio of discharge to charge capacities is the Coulomb efficiency that characterizes the excess energy required to charge the device. This excess energy is dissipated as heat. Therefore, high Coulomb efficiency, close to 100 % is desirable for any electrochemical device. Table 3 summarizes the Coulomb efficiencies of the ILs-based SCs. For all the electrolytes, an increase in Coulomb efficiency was observed with increasing the current density. At high current densities of 1–2.5 $A \cdot g^{-1}$ the Coulomb efficiencies exceed 80 %, which are suitable for electrochemical application. At the same time, a low current density of 0.2 $A \cdot g^{-1}$

Table 3. The Coulomb efficiency (%) of GNF- and N-GNF-based SCs at different current densities *i*

i, A·g^{-1}	GNFs					N-GNFs				
	0.2	1	1.5	2	2.5	0.2	1	1.5	2	2.5
No additive	84.6	95.5	96.7	97.3	97.8	88.1	97.7	98.5	98.8	99.1
0.01M Pyr11Fc	69.4	85.8	90.4	92.3	93.9	83.1	91.1	89.7	93.9	96.1
0.03M Pyr11Fc	41.8	78.6	85.3	88.8	91.1	55.2	83.9	89.1	92.1	93.7
0.05M Pyr11Fc	26.8	81.9	87.8	90.7	92.7	23.3	60.0	72.8	79.1	83.0
0.01M Pyr12Fc	76.2	91.4	94.1	95.5	96.4	87.0	95.1	96.8	97.7	98.2
0.03M Pyr12Fc	37.9	80.1	86.2	89.7	91.7	43.5	86.4	90.8	93.0	94.4
0.05M Pyr12Fc	29.3	78.7	85.5	89.2	91.5	27.5	84.7	85.0	89.1	91.4
0.01M Pip11Fc	83.2	93.9	95.7	96.7	97.3	83.1	94.6	96.5	97.4	98.0
0.03M Pip11Fc	43.1	82.3	87.6	90.8	92.6	51.2	87.8	89.4	89.5	86.3
0.05M Pip11Fc	35.4	81.6	87.0	90.4	92.2	42.4	81.7	87.6	90.6	92.4

led to significant drop in the Coulomb efficiencies of the Fc-ILs-based SCs down to 27 % probably because at low current density the rate of a potential leakage due to self-diffusion of the oxidized species to the anode was comparable with the rates of electric double layer accumulation and pseudo-capacitive processes. The similar result was reported by Bodin et al. [44] for the self-discharge of SCs based on 0.1 M of a 4-methylimidazolium-2,2,6,6-tetramethylpiperidine-1-oxyl bis(trifluoromethyl-sulfonyl)imide [TEMPOIm][NTf_2] redox-active IL in 1-butyl-3-methylimidazolium bis(trifluoromethyl-sulfonyl)imide [BMIm][NTf_2]. At a high current density of 0.5 A·g^{-1} the Coulomb efficiency of the SCs approached 100 %, while it significantly degraded at low current densities (< 0.1 A·g^{-1}).

The self-discharge rate is a crucial parameter for assessing performance and practical viability of SCs, as it directly impacts their energy retention capability. The self-discharge drop is usually described by several mechanisms [45–47]:

1) The self-discharge caused by redistribution of charge due to its non-uniform distribution on the surface and in the bulk of the electrode. In particular, after charging, ions gradually diffuse from the surface into the bulk material, decreasing the cell voltage.

2) The self-discharge controlled by a potential-dependent Faraday charge-transfer reaction (Fe^{2+}/Fe^{3+}):

$$E_t = E_0 - A\ln(t + t_0). \quad (5)$$

Here, A corresponds to Tafel slope constant, t is the time, t_0 is the integration constant, and E_0 is the initial cell potential.

3) The self-discharge determined by the semi-infinite diffusion of impurities within pores of the electrode material:

$$E_t = E_0 - 2zFSCc_0\sqrt{D\pi t}. \quad (6)$$

Here, D is the diffusion coefficient, S is the specific surface area of the porous electrode material, C is the cell capacitance.

4) The self-discharge caused by the leakage current flowing through a resistance between electrodes due to the imperfection of insulating materials used in the SC:

$$E_t = E_0 \exp\left(-\frac{t}{RC}\right). \quad (7)$$

Here, RC is the time constant of resistance.

In general, different mechanisms contribute to the self-discharge of SC. When the ohmic leakage is the main reason for self-discharge, a linear dependence between $\ln E_t$ and t is observed. In our case the $\ln E_t - t$ dependences are linear after discharging for approximately 10000 s (Fig. 3*a*). Also, experimental E_t versus $\ln(t)$ dependencies initially exhibit a plateau followed by a linear drop in the intermediate part of the self-discharge curves (Fig. 3*b*). When the self-discharge process is limited by diffusion in porous electrode, the voltage E_t should be proportional to the square root of the self-discharge time $t^{1/2}$. Such linear dependence is not observed for the Fc-ILs-based SCs (Fig. 3*c*), which excludes the significant effect of semi-infinite diffusion of impurities to a self-discharge. Therefore,

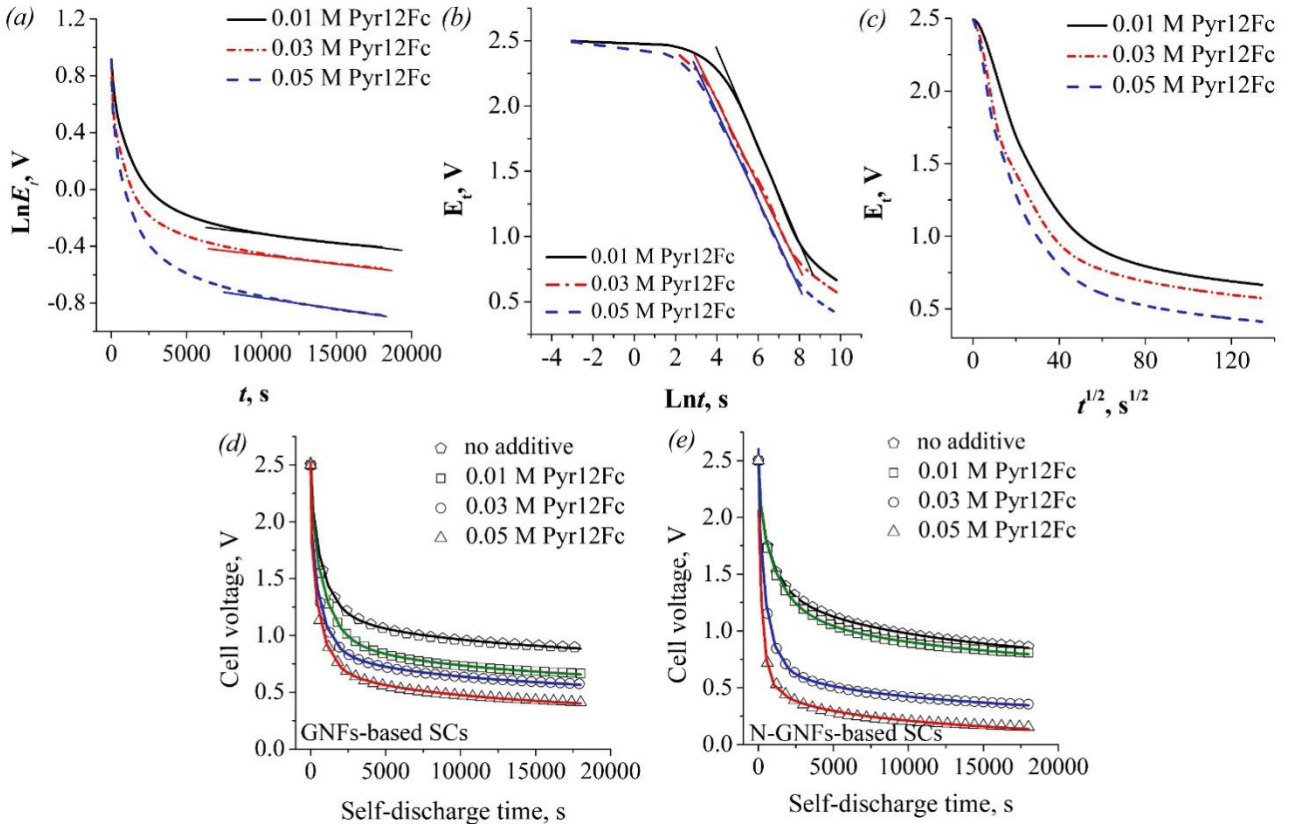

Fig. 3. Self-discharge profiles of SCs based GNFs and IL electrolyte with PyrFcEt additive as ln$E_t - t$ (*a*), E_t – ln$t$ (*b*) and $E_t - t^{1/2}$ (*c*), self-discharge profiles of GNF- (*d*) and N-GNF-based (*e*) SCs (Solid lines show the best-fit curves for hybrid model)

the initial drop in E_t after charging (Fig. 3*d*, *e*) attributed to the charge redistribution is followed by an activation-controlled process in the intermediate stage and, finally, by ohmic leakage, which agrees with data reported by Zhao et al. for all-solid-state SCs [48].

Faradaic redox processes and leakage-current mechanism mainly contribute to the self-discharge of the SCs. To account for the effects of both these mechanisms on self-discharge, the hybrid model was proposed:

$$E_t = A_0 - A_1 \ln(t + t_0) + A_2 \exp\left(-\frac{t}{RC}\right). \qquad (8)$$

Here, A_i is the fitting parameter. This model describes the experimental voltage drop versus time dependencies with high accuracy (coefficient of determination $R^2 > 0.997$) (Figs. 3*d*, *e*, Table 4).

In contrast to the SCs without redox-additives, the addition of Fc-ILs to the electrolyte enhances the rate of self-discharge due to the increased contribution of the "shuttle effect". Modification of the electrolytes with Fc-ILs leads to the formation of Fe^{3+} redox impurities. These species can migrate between two electrodes, where they are oxidized or reduced. The associated shuttle process causes a parasitic charge transfer, which lowers the SC voltage and increases its self-discharge rate. A similar trend was previously reported for the KOH/$K_3Fe(CN)_6$ [46] and Li_2SO_4/4-n-pentyl-4'-cyanobiphenyl [47] redox electrolytes.

The N-GNF-based SCs with the blank electrolyte showed a drop in the potential profile similar to that observed for GNFs-based SCs but with a higher self-discharge rate (Fig. 3*e*). Modification of carbon surface with nitrogen groups may facilitate adsorption of the oxidized species forming during Faradaic reactions. At the same time such products cannot quickly leave the electrode surface during self-discharge due to their strong interactions. In contrast to N-GNFs, adsorption of the oxidized species on the surface of undoped GNFs is weaker, which lowers their surface concentration and thus slows the self-discharge. Therefore, nitrogen-containing groups on the carbon surface don't facilitate self-discharge in the absence of redox impurities while redox-active electrolyte additives provide a shuttle of ferrocenyl-groups with their subsequent reduction on the cathode surface.

Table 4. Parameters of the best-fits to potential drop profiles with hybrid model (8)

Redox-electrolyte additive	$E_t = A_0 - A_1 \ln(t + t_0) + A_2 \exp\left(-\frac{t}{RC}\right)$					
	A_1, V	A_2, V	A_0, V	t_0, s	RC, s	R^2
			GNFs			
No additive	0.136 ± 0.001	0.708 ± 0.004	2.21 ± 0.01	14.7 ± 1.5	874 ± 7	0.9989
0.01M Pyr11Fc	0.124 ± 0.001	0.812 ± 0.008	1.85 ± 0.01	2.8 ± 0.5	495 ± 7	0.9979
0.03M Pyr11Fc	0.183 ± 0.001	0.404 ± 0.004	2.35 ± 0.01	2.9 ± 0.2	911 ± 11	0.9987
0.05M Pyr11Fc	0.129 ± 0.001	0.556 ± 0.008	1.92 ± 0.01	0.7 ± 0.1	503 ± 11	0.9970
0.01M Pyr12Fc	0.136 ± 0.001	0.821 ± 0.004	1.99 ± 0.01	6.4 ± 0.6	995 ± 6	0.9989
0.03M Pyr12Fc	0.123 ± 0.002	0.735 ± 0.009	1.77 ± 0.01	0.9 ± 0.2	720 ± 12	0.9972
0.05M Pyr12Fc	0.126 ± 0.001	0.800 ± 0.005	1.63 ± 0.01	0.5 ± 0.1	679 ± 6	0.9969
0.01M Pip11Fc	0.129 ± 0.001	0.834 ± 0.008	1.94 ± 0.01	6.2 ± 1.0	589 ± 8	0.9983
0.03M Pip11Fc	0.132 ± 0.001	0.794 ± 0.008	1.74 ± 0.01	1.1 ± 0.2	627 ± 9	0.9980
0.05M Pip11Fc	0.138 ± 0.001	0.684 ± 0.005	1.80 ± 0.01	0.6 ± 0.1	685 ± 8	0.9979
			N-GNFs			
No additive	0.184 ± 0.001	0.504 ± 0.002	2.60 ± 0.01	16.4 ± 0.6	1398 ± 6	0.9989
0.01M Pyr11Fc	0.153 ± 0.001	0.628 ± 0.003	2.12 ± 0.01	2.1 ± 0.2	626 ± 4	0.9963
0.03M Pyr11Fc	0.082 ± 0.001	1.373 ± 0.005	0.88 ± 0.01	0.04±0.01	211 ± 1	0.9911
0.05M Pyr11Fc	0.175 ± 0.001	0.398 ± 0.002	2.30 ± 0.01	1.4 ± 0.1	706 ± 6	0.9967
0.01M Pyr12Fc	0.215 ± 0.001	0.344 ± 0.001	2.96 ± 0.01	35.5 ± 0.6	963 ± 5	0.9995
0.03M Pyr12Fc	0.131 ± 0.001	1.031 ± 0.002	1.63 ± 0.01	1.6 ± 0.1	591 ± 1	0.9988
0.05M Pyr12Fc	0.125 ± 0.001	1.132 ± 0.004	1.37 ± 0.01	0.6 ± 0.1	282 ± 1	0.9945
0.01M Pip11Fc	0.239 ± 0.001	0.301 ± 0.001	3.19 ± 0.01	60.9 ± 0.5	1641 ± 5	0.9999
0.03M Pip11Fc	0.075 ± 0.001	1.371 ± 0.005	0.84 ± 0.01	0.02±0.01	176 ± 1	0.9896
0.05M Pip11Fc	0.129 ± 0.001	0.987 ± 0.002	1.56 ± 0.01	0.8 ± 0.1	471 ± 1	0.9988

Table 5. Energy ($Wh \cdot kg^{-1}$) [power ($kW \cdot kg^{-1}$)] densities of GNF- and N-GNF-based SCs

i, $A \cdot g^{-1}$	GNFs				N-GNFs			
	1	1.5	2	2.5	1	1.5	2	2.5
No additive	16.4 [1.1]	16.2 [1.7]	16.0 [2.4]	15.7 [2.9]	17.0 [1.1]	16.2 [1.7]	15.5 [2.2]	14.8 [2.7]
0.01M Pyr11Fc	17.7 [1.1]	17.5 [1.7]	17.0 [2.3]	16.9 [2.8]	18.0 [1.1]	17.1 [1.6]	16.3 [2.1]	15.5 [2.6]
0.03M Pyr11Fc	19.4 [1.1]	19.3 [1.7]	19.2 [2.3]	18.9 [2.9]	17.7 [0.9]	16.9 [1.4]	15.8 [1.9]	14.6 [2.3]
0.05M Pyr11Fc	23.1 [1.1]	23.0 [1.8]	22.9 [2.3]	22.6 [3.1]	18.8 [1.1]	18.0 [1.6]	17.1 [2.1]	16.3 [2.6]
0.01M Pyr12Fc	17.6 [1.2]	17.3 [1.7]	17.0 [2.5]	16.7 [2.9]	16.8 [1.1]	16.0 [1.6]	15.2 [2.1]	14.4 [2.6]
0.03M Pyr12Fc	21.2 [1.2]	21.2 [1.7]	21.1 [2.3]	20.8 [2.9]	17.2 [1.0]	16.4 [1.6]	15.59 [2.1]	14.8 [2.6]
0.05M Pyr12Fc	21.6 [1.1]	21.4 [1.7]	21.1 [2.4]	20.6 [2.9]	17.6 [1.1]	17.8 [1.5]	16.4 [2.0]	15.2 [2.4]
0.01M Pip11Fc	17.0 [1.1]	16.8 [1.8]	16.5 [2.4]	16.3 [2.9]	15.8 [1.1]	14.9 [1.6]	14.0 [2.1]	13.2 [2.5]
0.03M Pip11Fc	19.1 [1.2]	18.8 [1.7]	18.5 [2.4]	18.1 [2.9]	17.6 [0.9]	17.4 [1.4]	16.7 [1.9]	15.8 [2.4]
0.05M Pip11Fc	21.7 [1.1]	21.6 [1.8]	21.4 [2.4]	21.1 [2.9]	19.1 [1.1]	18.4 [1.6]	17.6 [2.1]	16.9 [2.6]

Specific energies and power densities were calculated from the GCD curves (Table 5). The highest E_{SC} values of 23.1, 21.6 and 21.7 Wh·kg^{-1} at P_{SC} of 1.2 kW·kg^{-1} were observed for the GNFs-based SCs with the supporting electrolyte 0.5 M [EMIm][NTf_2]/AN and 0.05 M Pyr11Fc, Pyr12Fc and Pip11Fc additives, respectively. For N-GNFs the energy densities were lower: 18.8 (0.05 M Pyr11Fc), 17.6 (0.05 M Pyr12Fc) and 19.1 (0.05 M Pip11Fc) Wh·kg^{-1}, which may be caused by higher impact of self-discharge. The specific energy densities of the Fc-ILs-based SCs were close to those previously reported for activated carbon in PVA/poly (vinyl pyrrolidone)/$EMIHSO_4$/HQ (24.3 Wh·kg^{-1} at ~1.5 kW·kg^{-1}) [5], PVA/Li_2SO_4/BMIMBr (38.0 Wh·kg^{-1} at 0.2 kW·kg^{-1}) [28], and PVA/Li_2SO_4/BMIMI (29.3 Wh·kg^{-1} at ~0.1 kW·kg^{-1}) [27], N-doped carbon in 2.5 M KBr + 2 M H_2SO_4 (14.3 Wh·kg^{-1} at 639.8 W·kg^{-1}) [20], reduced graphene oxide in H_2O/$K_4[Fe(CN)_6]$/K_2SO_4 (36.8 Wh·kg^{-1} at 1.2 kW·kg^{-1}) [16].

4. Conclusion

In summary, the ferrocene-containing ionic liquids were tested as new redox-additives to ILs electrolytes of non-aqueous supercapacitors with undoped and N-doped GNF electrodes. The electrochemical performance of the SCs was found to depend on the fraction of the redox-additive in 0.5 M [EMIm][NTf_2]/AN and the type of electrode material. Modification of 0.5 M [EMIm][NTf_2]/AN with 0.05 M Fc-ILs significantly improved the specific capacitance of the SCs due to reversible Faradaic reactions. Although nitrogen doping of GNFs was anticipated to enhance their pseudocapacitance, the results of our work demonstrate that changes in the textural parameter of GNFs under doping are the dominant factor affecting their specific capacitance in Fc-IL-based SCs. A self-discharge mechanism was analyzed using the hybrid model that accounts for contributions of charge redistribution, Faradaic redox processes and leakage-currents. In contrast to GNFs, N-GNFs negatively affected the SCs performance, increasing self-discharge due to the adsorption of redox-species on the electrode surface that was consistent with the decrease in Coulombic efficiencies (Table 3). Undoubtedly, this work demonstrates the promising performances of the Fc-ILs-based supercapacitors, however, a crucial role of the electrode material is highlighted.

5. Funding

This study was carried out with the financial support of the Russian Science Foundation (Project No. 24-23-00165).

Финансирование

Исследование выполнено за счет средств гранта Российского научного фонда № 24-23-00165.

6. Conflict of interests

The authors declare no conflict of interest.

Конфликт интересов

Авторы заявляют об отсутствии конфликта интересов.

References

1. Qin G, Liu Y, Zhang W, He W, et al. Integrated supercapacitor with self-healing, arbitrary deformability and anti-freezing based on gradient interface structure from electrode to electrolyte. *Journal of Colloid and Interface Science*. 2023;635:427-440. DOI:10.1016/j.jcis.2022.12.164

2. Hor AA, Yadav N, Hashmi SA. High energy density carbon supercapacitor with ionic liquid-based gel polymer electrolyte: role of redox-additive potassium iodide. *Journal of Energy Storage*. 2022;47:103608. DOI:10.1016/j.est.2021.103608

3. Arsha MS, Biju V. A 3.5 V supercapacitor with ultrahigh energy and power capabilities using thermally deoxygenated graphite oxide electrodes and water-in-salt electrolyte. *Energy & Fuels*. 2024;38(19):19076-19087. DOI:10.1021/acs.energyfuels.4c02984

4. Hao L, Shen L, Wang J, Xu Y, et al. Hollow $NiCo_2S_4$ nanotube arrays grown on carbon textile as a self-supported electrode for asymmetric supercapacitors. *RSC Advances*. 2016;6(12):9950-9957. DOI:10.1039/C5RA24068A

5. Yadav N, Yadav N, Hashmi SA. Ionic liquid incorporated, redox-active blend polymer electrolyte for high energy density quasi-solid-state carbon supercapacitor. *Journal of Power Sources*. 2020;451:227771. DOI:10.1016/j.jpowsour.2020.227771

6. Luo Y, Wang S, Xu Y, Liu N, et al. Exploring redox-active electrolytes to boost energy density of carbon-based supercapacitors. *Journal of Colloid and Interface Science*. 2025;684:729-734. DOI:10.1016/j.jcis.2025.01.082

7. Halder J, De P, Chandra A. Synergistic contribution of redox additive electrolytes to significantly increase the performances of hybrid supercapacitors. *Journal of Energy Storage*. 2024;104:114583. DOI:10.1016/j.est.2024.114583

8. Arkhipova EA, Ivanov AS, Isaikina OYa, Novotortsev RYu, et al. Application of MnO_2/MWCNT composite in supercapacitors. *Materials Today: Proceedings*. 2022;60:1008-1011. DOI:10.1016/j.matpr.2021.12.408

9. Shanmugavani A, Kaviselvi S, Sankar KV, Selvan RK. Enhanced electrochemical performances of PANI using redox additive of $K_4[Fe(CN)_6]$ in aqueous electrolyte for symmetric supercapacitors. *Materials Research Bulletin*. 2015;62:161-167. DOI:10.1016/j.materresbull.2014.10.075

10. Arkhipova EA, Ivanov AS, Maslakov KI, Savilov SV. Nitrogen-doped mesoporous graphene nanoflakes for high performance ionic liquid supercapacitors. *Electrochimica Acta*. 2020;353:136463. DOI:10.1016/j.electacta.2020.136463

11. Kumar R, Sahoo S, Joanni E, Singh RK, et al. Heteroatom doped graphene engineering for energy storage and conversion. *Materials Today*. 2020;39:47-65. DOI:10.1016/j.mattod.2020.04.010

12. Śliwak A, Grzyb B, Díez N, Gryglewicz G. Nitrogen-doped reduced graphene oxide as electrode material for high-rate supercapacitors. *Applied Surface Science*. 2017;399:265-271. DOI:10.1016/j.apsusc.2016.12.060

13. Chen Y, Huang J, Zhang X, Xu H. Fabrication of hybrid supercapacitor of RGO//PPyNTs/$Co(OH)_2$ based on $K_3Fe(CN)_6$ redox-active electrolyte. *Journal of Electroanalytical Chemistry*. 2021;884:115069. DOI:10.1016/j.jelechem.2021.115069

14. Akhtar MA, Chowdhury A, Chandra A. Addition of redox additives–synergic strategy for enhancing the electrochemical activity of spinel Co_3O_4 based supercapacitors. *Journal of Physics D: Applied Physics*. 2019;52(15):155501. DOI:10.1088/1361-6463/ab00d3

15. Oskin P, Lepikash R, Dyachkova T, Alferov S. Comparative evaluation of different methods for determining the specific surface area of carbon materials used in electrochemical systems. *Journal of Advanced Materials and Technologies*. 2024;9(3):167-176. DOI:10.17277/jamt.2024.03.pp.167-176

16. Sawant SA, Waikar MR, Chodankar GR, Gurav SR, et al. A redox additive electrolyte boosted supercapacitive energy density of wrinkled RGO sheets. *Journal of Energy Storage*. 2024;76:109739. DOI:10.1016/j.est.2023.109739

17. Raja TA, Vickraman P. Role of dual redox additives KI/ $VOSO_4$ in manganese ammonium phosphate at graphene quantum dots for supercapattery. *International Journal of Energy Research*. 2022;46(7):9097-9113. DOI:10.1002/er.7787

18. Yang W, Han Q, Li W, Wu M, et al. Suppressed shuttle effect and Self-Discharge of redox electrochemical capacitors using biphasic electrolyte with a Liquid-Liquid interface. *Chemical Engineering Journal*. 2022;448:137731. DOI:10.1016/j.cej.2022.137731

19. Fic K, Morimoto S, Frąckowiak E, Ishikawa M. Redox activity of bromides in carbon-based electrochemical capacitors. *Batteries & Supercaps*. 2020;3(10):1080-1090. DOI:10.1002/batt.202000061

20. Hwang B, Yang J, Kim D, Yun WC, et al. Redox enhanced membraneless electrochemical capacitor with CO_2-derived hierarchical porous carbon electrodes. *Electrochimica Acta*. 2023;442:141871. DOI:10.1016/j.electacta.2023.141871

21. Liu Y, Dai J, Xiao Y, Wang Y, et al. Novel zinc-ion hybrid supercapacitors with enhanced specific capacity by redox-active ions. *Journal of Energy Storage*. 2024;77:109834. DOI:10.1016/j.est.2023.109834

22. Huang X, Wang Q, Chen XY, Zhang ZJ. The effects of amine/nitro/hydroxyl groups on the benzene rings of redox additives on the electrochemical performance of carbon-based supercapacitors. *Physical Chemistry Chemical Physics*. 2016;18(15):10438-10452. DOI:10.1039/C6CP00211K

23. Manickavasakam K, Suresh Balaji S, Kaipannan S, Karthick Raj AG, et al. Electrochemical performance of Thespesia Populnea seeds derived activated carbon – supercapacitor and its improved specific energy in redox additive electrolytes. *Journal of Energy Storage*. 2020;32:101939. DOI:10.1016/j.est.2020.101939

24. Gebremariam GK, Jovanović AZ, Pašti IA. The effect of electrolytes on the kinetics of the hydrogen evolution reaction. *Hydrogen*. 2023;4(4):776-806. DOI:10.3390/hydrogen4040049

25. Warrington A, O'Dell LA, Hutt OE, Forsyth M, et al. Structure and interactions of novel ether-functionalised morpholinium and piperidinium ionic liquids with lithium salts. *Energy Advances*. 2023;2(4):530-546. DOI:10.1039/D2YA00348A

26. Ong SP, Andreussi O, Wu Y, Marzari N, et al. Electrochemical windows of room-temperature ionic liquids from molecular dynamics and density functional theory calculations. *Chemistry of Materials*. 2011;23(11):2979-2986. DOI:10.1021/cm200679y

27. Tu QM, Fan LQ, Pan F, Huang JL, et al. Design of a novel redox-active gel polymer electrolyte with a dual-role ionic liquid for flexible supercapacitors. *Electrochimica Acta*. 2018;268:562-568. DOI:10.1016/j.electacta.2018.02.008

28. Fan LQ, Tu QM, Geng CL, Huang JL, et al. High energy density and low self-discharge of a quasi-solid-state supercapacitor with carbon nanotubes incorporated redox-active ionic liquid-based gel polymer electrolyte. *Electrochimica Acta*. 2020;331:135425. DOI:10.1016/j.electacta.2019.135425

29. Lee KS, Jeong HT. Development and optimization of ionic liquid-based gel polymer electrolyte for all solid-state supercapacitor. *Journal of Energy Storage*. 2021;42:103001. DOI:10.1016/j.est.2021.103001

30. Geng CL, Fan LQ, Wang CY, Wang YL, et al. High energy density and high working voltage of a quasi-solid-state supercapacitor with a redox-active ionic liquid added gel polymer electrolyte. *New Journal of Chemistry*. 2019;43(47):18935-18942. DOI:10.1039/C9NJ04769G

31. Benjamin M, Manoj D, Karnan M, et al. Switching the solubility of electroactive ionic liquids for designing high energy supercapacitor and low potential biosensor. *Journal of Colloid and Interface Science*. 2021;588:221-231. DOI:10.1016/j.jcis.2020.12.033

32. Xie HJ, Gélinas B, Rochefort D. Redox-active electrolyte supercapacitors using electroactive ionic liquids. *Electrochemistry Communications*. 2016;66:42-45. DOI:10.1016/j.elecom.2016.02.019

33. Borchers PS, Gerlach P, Liu Y, Hager MD, et al. The influence of the nature of redox-active moieties on the properties of redox-active ionic liquids and on their use as electrolyte for supercapacitors. *Energies*. 2021;14(19): 6344. DOI:10.3390/en14196344

34. Gélinas B, Forgie JC, Rochefort D. Conductivity and electrochemistry of ferrocenyl-imidazolium redox ionic liquids with different alkyl chain lengths. *Journal of The Electrochemical Society*. 2014;161(4):H161-H165. DOI:10.1149/2.017404jes

35. Arkhipova EA, Levin MM, Ivanov AS, Zakharov MA, et al. Electroactive ferrocene-based ionic liquids: transport and electrochemical properties of their acetonitrile solutions. *Electrochimica Acta*. 2025;512:145443. DOI:10.1016/j.electacta.2024.145443

36. Arkhipova EA, Ivanov AS, Maslakov KI, Egorov AV, et al. Mesoporous graphene nanoflakes for high performance supercapacitors with ionic liquid electrolyte. *Microporous and Mesoporous Materials*. 2020;294:109851. DOI:10.1016/j.micromeso.2019.109851

37. Savilov SV, Arkhipova EA, Ivanov AS, Maslakov KI, et al. Pyrolytic synthesis and characterization of N-doped carbon nanoflakes for electrochemical applications. *Materials Research Bulletin*. 2015;69:7-12. DOI:10.1016/j.materresbull.2014.12.057

38. Klein JM, Panichi E, Gurkan B. Potential dependent capacitance of [EMIM][TFSI], [N_{1114}][TFSI] and [PYR_{13}][TFSI] ionic liquids on glassy carbon. *Physical Chemistry Chemical Physics*. 2019;21(7):3712-3720. DOI:10.1039/C8CP04631J

39. Choudhury BJ, Muigai HH, Kalita P, Moholkar VS. Biomass blend derived porous carbon for aqueous supercapacitors with commercial-level mass loadings and enhanced energy density in redox-active electrolyte. *Applied Surface Science*. 2022;601:154202. DOI:10.1016/j.apsusc.2022.154202

40. Ghosh K, Srivastava SK. Enhanced supercapacitor performance and electromagnetic interference shielding effectiveness of CuS quantum dots grown on reduced graphene oxide sheets. *ACS Omega*. 2021;6(7):4582-4596. DOI:10.1021/acsomega.0c05034

41. Duraisamy N, Arshid N, Kandiah K, Iqbal J, et al. Development of asymmetric device using $Co_3(PO_4)_2$ as a positive electrode for energy storage application. *Journal of Materials Science: Materials in Electronics*. 2019;30(8):7435-7446. DOI:10.1007/s10854-019-01057-x

42. Zhou D, Wang H, Mao N, Chen Y, et al. High energy supercapacitors based on interconnected porous carbon nanosheets with ionic liquid electrolyte. *Microporous and Mesoporous Materials*. 2017;241:202-209. DOI:10.1016/j.micromeso.2017.01.001

43. Lee J, Srimuk P, Fleischmann S, Su X, et al. Redox-electrolytes for non-flow electrochemical energy storage: a critical review and best practice. *Progress in Materials Science*. 2019;101:46-89. DOI:10.1016/j.pmatsci.2018.10.005

44. Bodin C, Sekhar Bongur C, Deschanels M, Catrouillet S, et al. Shuttle effect quantification for redox ionic liquid electrolyte correlated to the coulombic efficiency of supercapacitors. *Batteries & Supercaps*. 2020;3(11):1193-1200. DOI:10.1002/batt.202000084

45. Shang W, Yu W, Xiao X, Ma Y, et al. Insight into the self-discharge suppression of electrochemical capacitors: progress and challenges. *Advanced Powder Materials.* 2023;2(1):100075. DOI:10.1016/j.apmate.2022.100075

46. Chen H, Zhang Y, Yang H, Jia B, et al. Self-discharge of redox electrolyte enhanced supercapacitors based on nanosheet-like CoS_2. *Chemical Engineering Journal*. 2024;494:152910. DOI:10.1016/j.cej.2024.152910

47. Volfkovich YuM. Self-discharge of supercapacitors: a review. *Russian Journal of Electrochemistry*. 2023;59(1):24-36. DOI:10.1134/S1023193523010123

48. Zhao H, Zhang H, Wang Z, Jiang X, et al. Chain-Elongated ionic liquid electrolytes for low self-discharge all-solid-state supercapacitors at high temperature. *ChemSusChem*. 2021;14(18):3895-3903. DOI:10.1002/cssc.202101294

Information about the authors / Информация об авторах

Mikhail M. Levin, Technician, Lomonosov Moscow State University (MSU), Faculty of Chemistry, Moscow, Russian Federation; ORCID 0000-0003-1156-2159; e-mail: mikhail.levin@chemistry.msu.ru

Ekaterina A. Arkhipova, Cand. Sc. (Chem.), Senior Researcher, MSU, Faculty of Chemistry, Moscow, Russian Federation; ORCID 0000-0002-1710-2041; e-mail: ekaterina.a.arkhipova@gmail.com

Anton S. Ivanov, Cand. Sc. (Chem.), Senior Researcher, MSU, Faculty of Chemistry, Moscow, Russian Federation; ORCID 0000-0003-1719-0106; e-mail: anthon.s.ivanov@gmail.com

Левин Михаил Михайлович, техник, Московский государственный университет им. М. В. Ломоносова (МГУ), Химический факультет, Москва, Российская Федерация; ORCID 0000-0003-1156-2159; e-mail: mikhail.levin@chemistry.msu.ru

Архипова Екатерина Анатольевна, кандидат химических наук, старший научный сотрудник, МГУ, Химический факультет, Москва, Российская Федерация; ORCID 0000-0002-1710-2041; e-mail: ekaterina.a.arkhipova@gmail.com

Иванов Антон Сергеевич, кандидат химических наук, старший научный сотрудник, МГУ, Химический факультет, Москва, Российская Федерация; ORCID 0000-0003-1719-0106; e-mail: anthon.s.ivanov@gmail.com

Konstantin I. Maslakov, Cand. Sc. (Phys. and Math.), Senior Researcher, MSU, Faculty of Chemistry, Moscow, Russian Federation; ORCID 0000-0002-0672-2683; e-mail: nonvitas@gmail.com

Serguei V. Savilov, D. Sc. (Chem.), Associate Professor, Leading Researcher, MSU, Faculty of Chemistry, Moscow, Russian Federation; ORCID 0000-0002-5827-3912; e-mail: savilov@mail.ru

Маслаков Константин Игоревич, кандидат физико-математических наук, старший научный сотрудник, МГУ, Химический факультет, Москва, Российская Федерация; ORCID 0000-0002-0672-2683; e-mail: nonvitas@gmail.com

Савилов Сергей Вячеславович, доктор химических наук, доцент, ведущий научный сотрудник, МГУ, Химический факультет, Москва, Российская Федерация; ORCID 0000-0002-5827-3912; e-mail: savilov@mail.ru

Received 03 November 2025; Revised 08 December 2025; Accepted 09 December 2025